nature neuroscience

Supplementary information

https://doi.org/10.1038/s41593-026-02389-8

State-dependent signal flow hierarchy in the human cerebral cortex

In the format provided by the authors and unedited

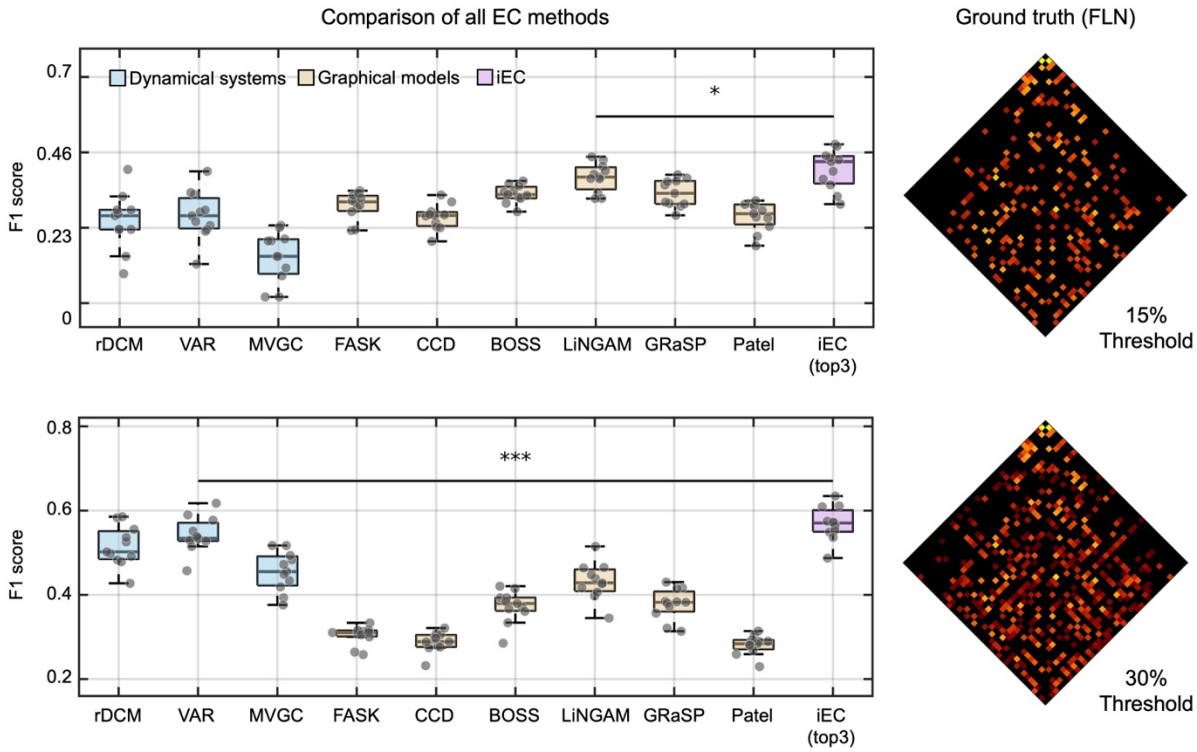

Supplementary Fig. 1 | F1 scores of EC algorithms. F1 scores were computed after binarizing both the estimated EC matrices and the ground-truth FLN matrix at the top 15% (upper panel) or 30% (lower panel) of absolute connection strengths. The y axis shows F1 score and the x axis lists the individual algorithms and iEC. Each dot represents one macaque fMRI dataset in the independent test set (n=10 macaque datasets per algorithm and threshold); box plots are overlaid on the dots. Blue, beige, and purple denote dynamical-systems algorithms, graphical-model algorithms, and iEC, respectively. Matrices at right show the thresholded FLN used as ground truth for the corresponding sparsity level. Horizontal bars indicate the comparison between iEC (top3) and the best-performing individual algorithm (Wilcoxon test, $P = 1.0 \times 10^{-2}$ for the 15% threshold and $P = 4.8 \times 10^{-4}$ for the 30% threshold).

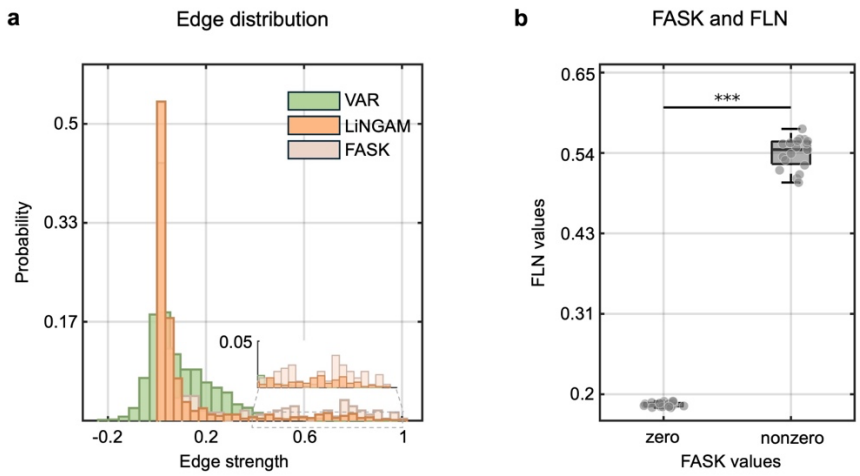

Supplementary Fig. 2 | Distinct output profiles of EC algorithms. a. Edge-weight distributions for three representative algorithms. The x axis shows edge strength and the y axis shows probability. Green, orange, and pale-pink histograms correspond to VAR, LiNGAM, and FASK, respectively; the inset magnifies the sparse upper-tail regime. b, Comparison of FLN values for connections classified by FASK as absent (zero) or present (nonzero). The x axis shows the FASK classification and the y axis shows FLN value. Each dot represents one macaque fMRI dataset (n=10 macaque datasets); box plots are overlaid on the dots. Nonzero FASK connections showed higher FLN values than zero FASK connections (Wilcoxon rank-sum test, $P = 2.37 \times 10^{-7}$).

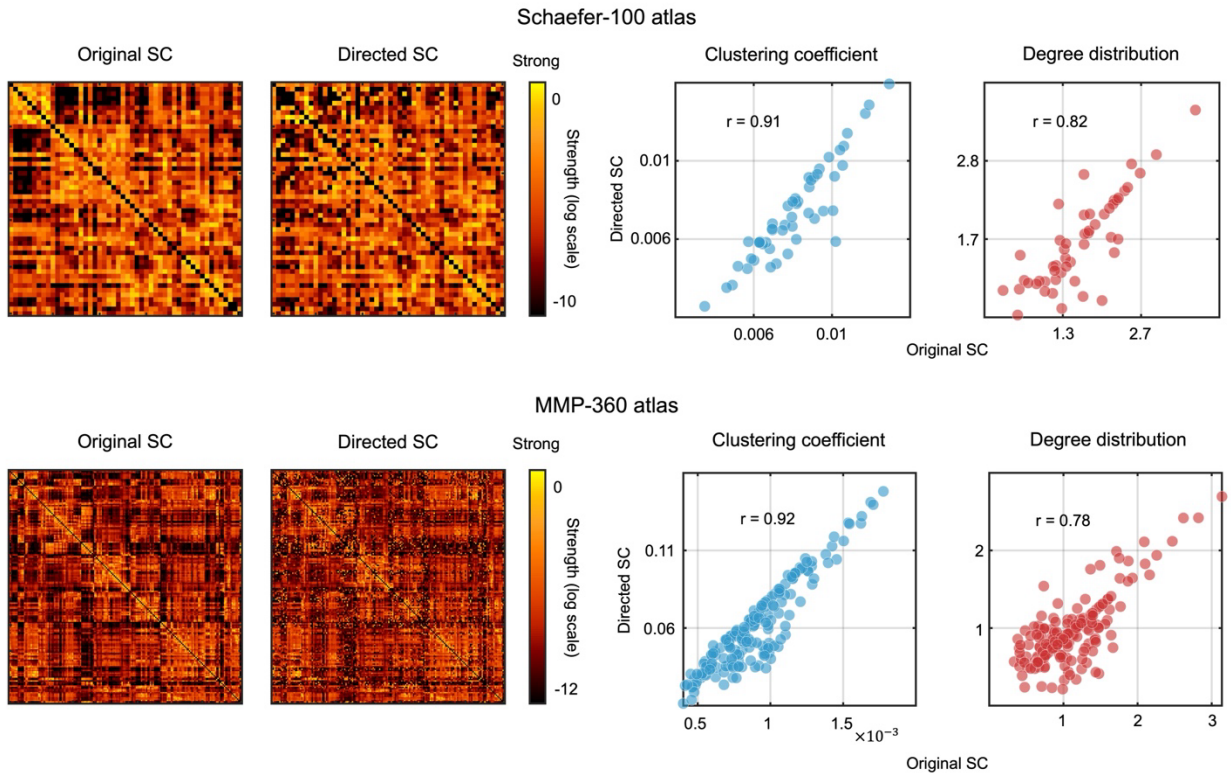

Supplementary Fig. 3 | Comparison between original and synthetic (directed) SC. Group-averaged structural connectivity (SC) matrices derived from diffusion MRI of 86 HCP participants are shown for the left hemisphere only (upper row, Schaefer-100 atlas; lower row, MMP-360 atlas). Connection strengths were log-transformed for visualization, and the heat-map color bars indicate log-transformed connection strength. For each atlas, the left heat map shows the original SC and the middle heat map shows the synthetic directed SC generated with the randmio_dir_connected algorithm. The right-hand scatter plots compare parcel-wise clustering coefficient (blue) and degree distribution (red) between the original and directed SC matrices; each point represents one left-hemisphere parcel (n=50 parcels for Schaefer-100; n=180 parcels for MMP-360). Pearson correlations are shown in each panel (Schaefer-100: $r = 0.91$ for clustering coefficient and $r = 0.82$ for degree distribution; MMP-360: $r = 0.92$ and $r = 0.78$, respectively).

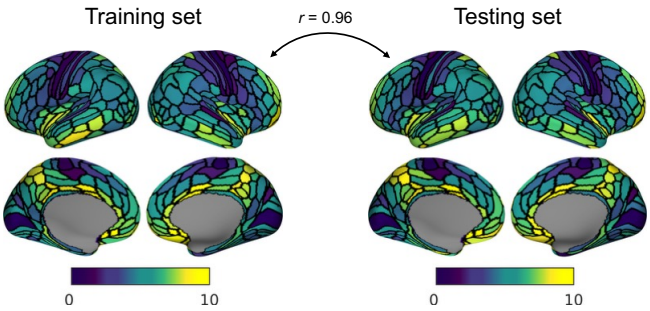

Supplementary Fig. 4 | Replicability of cortical hierarchy maps across independent training and testing sets. Cortical hierarchy maps derived from iEC were estimated independently in the training and testing HCP resting-state datasets (n=220 participants per set). For each map, iEC was constructed using β values optimized in the opposite dataset (training β applied to testing data, and vice versa). The four surface views show lateral and medial views of both hemispheres. Colour bars indicate hierarchy level (0–10). The arrow and r value denote the parcel-wise Pearson correlation between the two maps ($r = 0.96$), indicating high replicability across datasets.

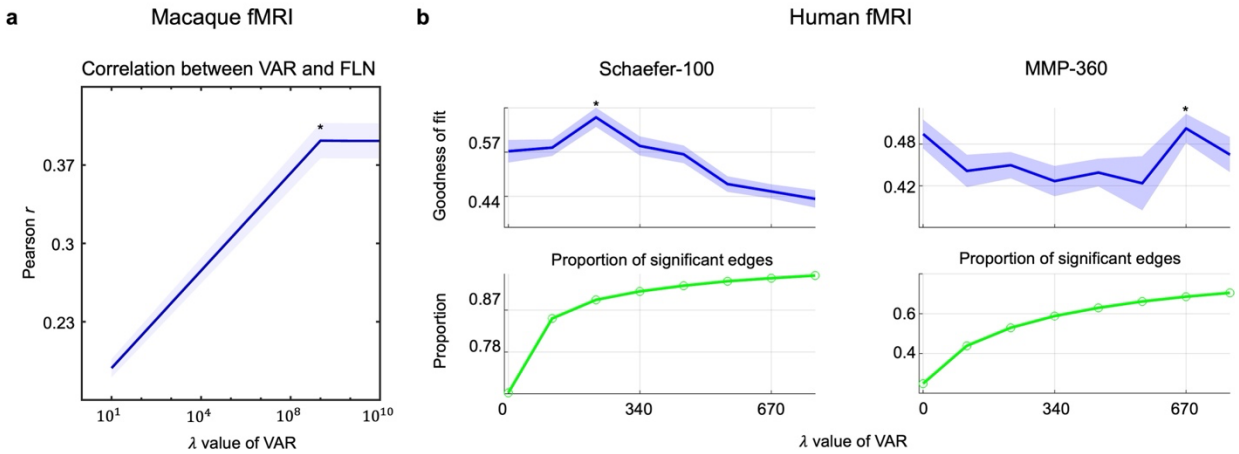

Supplementary Fig. 5 | Optimization of the regularization parameter (λ) in the VAR algorithm using ground-truth and empirical data. a, Training macaque fMRI data (n=9 macaque datasets) were used to select λ by maximizing the correlation between VAR-estimated EC and the ground-truth FLN matrix. The x axis shows λ (log scale) and the y axis shows Pearson's r. The blue line shows the correlation across λ values, and the correlation plateaued at high λ ($\lambda > 10^8$). **b**, , Human training data (n=220 participants) were used to optimize λ by maximizing the overall fit between simulated and empirical brain activity for the Schaefer-100 and MMP-360 atlases. In the top row, the x axis shows λ and the y axis shows goodness of fit; blue lines show the fit curves and blue shaded bands indicate variability around the curves. In the bottom row, green lines show the corresponding proportion of significant edges. Asterisks mark the λ values yielding the peak overall fit.

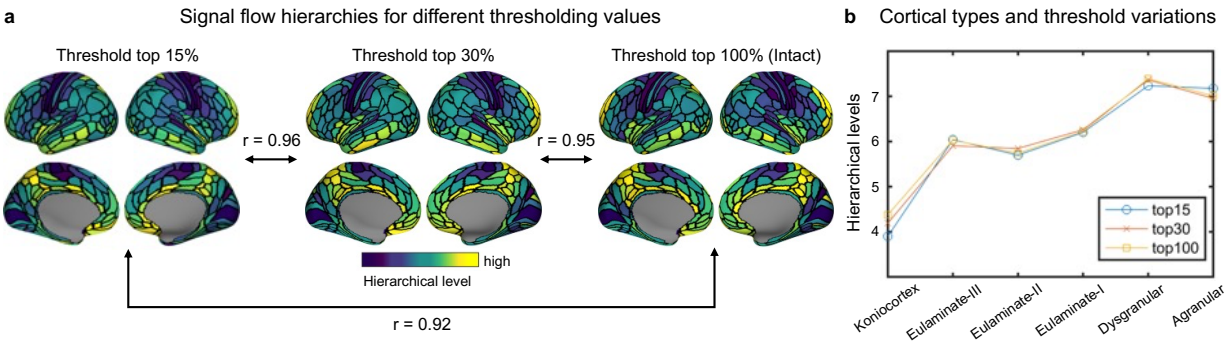

Supplementary Fig. 6 | Comparison of signal flow hierarchies for different threshold values. a, Using the group-level resting-state iEC map from the HCP testing dataset (n=220 participants), signal-flow hierarchy maps were derived after thresholding at the top 15%, 30%, or 100% of absolute edge weights. Surface maps show lateral and medial views of both hemispheres; the colour bar indicates hierarchical level from low to high. Arrows and r values denote parcel-wise Pearson correlations between the maps (15% vs 30%, $r = 0.96$; 30% vs 100%, $r = 0.95$; 15% vs 100%, $r = 0.92$). b, median hierarchy values are plotted for each cortical type. The x axis lists cortical types and the y axis shows hierarchical level. Blue, green, and orange lines correspond to the top15, top30, and top100 thresholded maps, respectively. The close overlap of the curves indicates that the estimated signal-flow hierarchy is robust to the choice of network threshold.